Atmospheric Environment 89 (2014) 52–63

Contents lists available at ScienceDirect

Atmospheric Environment

journal homepage: www.elsevier.com/locate/atmosenv

Development and evaluation of the unified tropospheric–stratospheric chemistry extension (UCX) for the global chemistry-transport model GEOS-Chem

Sebastian D. Eastham [a], Debra K. Weisenstein [b], Steven R.H. Barrett [a,*]

[a] Laboratory for Aviation and the Environment, Department of Aeronautics and Astronautics, Massachusetts Institute of Technology, Cambridge, MA 02139, USA

[b] Harvard School of Engineering and Applied Sciences, 29 Oxford Street, Cambridge, MA 02138, USA

HIGHLIGHTS

- We extend GEOS-Chem with a unified tropospheric–stratospheric chemical mechanism.
- Emission, transport, mixed-phase chemistry, photolysis and destruction of new species.
- Fast-JX couples online stratospheric aerosols to tropospheric photochemistry.
- Models 90% of maximum ozone depletion in 2006 Antarctic ozone hole.
- Widely-used model now captures coupled stratospheric–tropospheric responses.

ARTICLE INFO

Article history:
Received 25 September 2013
Received in revised form
30 January 2014
Accepted 4 February 2014
Available online 6 February 2014

Keywords:
GEOS-Chem
Stratospheric chemistry
Ozone hole
Model development
Model validation

ABSTRACT

Global chemistry-transport models (CTMs) typically use simplified parameterizations or relaxation to climatology to estimate the chemical behavior of the stratosphere only in the context of its impact on tropospheric chemistry. This limits investigation of stratospheric chemistry and interactions between tropospheric and stratospheric chemistry-transport processes. We incorporate stratospheric chemical and physical processes into the model GEOS-Chem in the form of a unified chemistry extension (UCX). The stratospheric chemistry framework from NASA's Global Modeling Initiative (GMI) is updated in accordance with JPL 10-06 and combined with GEOS-Chem's existing widely applied and validated tropospheric chemistry to form a single, unified gas-phase chemistry scheme. Aerosol calculations are extended to include heterogeneous halogen chemistry and the formation, sedimentation and evaporation of polar stratospheric clouds (PSCs) as well as background liquid binary sulfate (LBS) aerosols. The Fast-JX v7.0a photolysis scheme replaces a hybrid of Fast-J and Fast-JX v6.2, allowing photolytic destruction at frequencies relevant to the stratosphere and of species not previously modeled. Finally, new boundary conditions are implemented to cover both surface emissions of new species and mesospheric behavior. Results for four simulation years (2004–2007) are compared to those from the original, tropospheric model and to in situ and satellite-based measurements. We use these comparisons to show that the extended model is capable of modeling stratospheric chemistry efficiently without compromising the accuracy of the model at lower altitudes, perturbing mean OH below 250 hPa by less than 5% while successfully capturing stratospheric behavior not previously captured in GEOS-Chem such as formation and collapse of the Antarctic ozone hole. These extensions (with supporting validation and intercomparison) enable an existing and extensively validated tropospheric CTM to be used to investigate a broader set of atmospheric chemistry problems and leverages GEOS-Chem's existing tropospheric treatment.

1. Introduction

GEOS-Chem is a three-dimensional global tropospheric chemical-transport model (CTM) initially developed at Harvard University in the late 1990s (Bey et al., 2001) and collaboratively

* Corresponding author.
E-mail address: sbarrett@mit.edu (S.R.H. Barrett).

http://dx.doi.org/10.1016/j.atmosenv.2014.02.001
1352-2310/

Table 1
Comparison of existing models to GEOS-Chem UCX. Models with distinct chemical mechanisms for the troposphere and stratosphere are shown here with two counts (tropospheric/stratospheric). Although GEOS-Chem can be run with secondary organic aerosols (SOA), these are not modeled in the default setup.

	Species	Kinetic reactions	Photolysis reactions	Soot	Organic carbon	Dust	Tropospheric sulfates	SOA	Sea salt	Stratospheric aerosols	Focus region
GC UCX	132	344	89	2	2	7	Y	Y/N	2	2	T, S
GEOS-Chem[a]	104	240	55	2	2	7	Y	Y/N	2	0	T
CAM-chem[b]	117	263	69	2	2	4	Y	Y	4	4	T
MOZART-3[c]	108	236	71	2	2	0	Y	Y	4	4	T, S, M
MOZART-4[d]	85	161	39	2	2	4	Y	Y	4	0	T
TM-5[e]	42	64	16	0	0	0	Y	N	0	0	T, S
GMI[f]	46	116	38	1	0	0	N	N	0	4	T, S
OSLO CTM3[g]	97	88/112	17/47	4	4	2	Y	Y	8	3	T, S
TOMCAT[h]	41	93	25	0	0	0	N	N	0	0	T
SLIMCAT[i]	43	109	29	0	0	0	N	N	0	3	S
CMAM[j]	44	93	34	0	0	0	N	N	0	1	S, M

[a] Bey et al., 2001.
[b] Lamarque et al., 2012.
[c] Kinnison et al., 2007.
[d] Emmons et al., 2010.
[e] Huijnen et al., 2010.
[f] Considine et al., 2000; Rotman and Tannahill, 2001.
[g] Søvde et al., 2012.
[h] Arnold et al., 2005.
[i] Chipperfield, 2006.
[j] De Grandpré et al., 2000.

updated since (http://www.geos-chem.org). It has seen widespread use for investigations of the atmospheric response to emissions and natural phenomena (Barkley et al., 2011; Duncan Fairlie et al., 2007; Mao et al., 2010). The bulk of chemical reactions are accounted for only within the troposphere. Stratospheric chemistry is approximated through two primary mechanisms. The linearized ozone (Linoz) method (McLinden et al., 2000) is employed to estimate stratospheric ozone concentrations. Stratospheric bromine species concentrations are specified from climatology (Parrella et al., 2012). The evolution of most other species in the stratosphere is calculated based on archived monthly mean production rates and loss frequencies from NASA's Global Modeling Initiative (GMI) code (Murray et al., 2012; Rotman et al., 2001).

We develop the GEOS-Chem tropospheric–stratospheric unified chemistry extension (UCX) to include stratospheric chemistry in GEOS-Chem, thus enabling capture of stratospheric responses and troposphere–stratosphere coupling. Additionally, investigations of chemical feedbacks between stratospheric ozone and aerosols and tropospheric photochemistry are made possible through extension of photolysis to the stratopause, calculation of J-values for shorter wavelengths and improved modeling of high-altitude aerosols.

The paper is structured as follows: Section 2 outlines the changes and extensions which have been applied to GEOS-Chem with the aim of producing an accurate, unified model of the troposphere and stratosphere. Section 3 intercompares the results from the extended model against existing model results and validates against historical observations, with conclusions summarized in Section 4. The purpose of these extensions (with supporting validation and intercomparison) is to enable an existing and extensively validated community tropospheric CTM to be used to investigate a broader set of atmospheric chemistry problems, while leveraging the tropospheric chemistry of GEOS-Chem.

2. Model description

The base model is GEOS-Chem version 9-01-03. The extended (UCX) version models 132 chemical species, with long-lived chemical families transported in 54 tracers. For the simulations presented in this paper, we use GEOS-5 meteorological fields from NASA's Global Modeling and Assimilation Office (GMAO) over 72 hybrid sigma-eta pressure levels extending from the surface to 0.01 hPa. For computational efficiency we employ a $4^\circ \times 5^\circ$ horizontal resolution, although the model can be driven at higher resolutions including nested grid modeling at (for example) $0.5^\circ \times 0.667^\circ$ (Barkley et al., 2011). The UCX makes no changes to the global transport, convection or mixing processes.

Table 1 shows the relative scope of GEOS-Chem with and without the UCX, along with some other existing models. The "Focus Region" column corresponds to the part of the atmosphere—troposphere, stratosphere, mesosphere or a combination – is the primary focus of the model.

2.1. Chemistry

The UCX extends the chemistry mechanism to include reactions relevant to the stratosphere. As shown in Table 1, we add 28 species and 104 kinetic reactions, including 8 heterogeneous reactions, along with 34 photolytic decompositions. These were identified by comparing reactions and processes already present to those included in the GMI stratospheric chemistry mechanism (Rotman et al., 2001). Reaction constants were updated in line with JPL 10-06 (Sander et al., 2011). A full listing of modeled species and reactions is given in the Supplementary information (SI), available online.

2.1.1. Gas-phase kinetic chemistry

We explicitly model atomic oxygen [both $O(^3P)$ and $O(^1D)$]. The base model neglects them as intermediates due to their short lifetimes. Although these species still exhibit short lifetimes in the stratosphere, their importance in correctly modeling stratospheric chemistry result in the need for these reactions to be explicitly considered. We also explicitly model ground state atomic hydrogen (H) and nitrogen (N) as active species.

We also combine GEOS-Chem's bromine mechanism (Parrella et al., 2012) with an adapted version of GMI's chlorine mechanism. Chlorine is transported to the stratosphere in long-lived organic species such as CFCs and HCFCs, followed by the release of active chlorine and subsequent sequestration in reservoir species ($ClONO_2$ and HCl). Halon species H-1211, H-1301 and H-2402 are added as organic sources of bromine. Heterogeneous halogen chemistry is also modeled (see Section 2.1.3). Dry deposition and

wet scavenging of HCl is modeled by assuming similar behavior to HBr, using a large Henry's law coefficient to yield near-100% uptake.

2.1.2. Photochemistry

GEOS-Chem uses a customized version of the Fast-JX v6.2 photolysis rate solver (Wild et al., 2000), which efficiently estimates tropospheric photolysis. The customized version uses the wavelength bands from the older Fast-J tropospheric photolysis scheme and does not consider wavelengths shorter than 289 nm, assuming they are attenuated above the tropopause. However, these high-energy photons are responsible for the release of ozone-depleting agents in the stratosphere. The standard Fast-JX model (Prather, 2012) addresses this limitation by expanding the spectrum analyzed to 18 wavelength bins covering 177–850 nm, extending the upper altitude limit to approximately 60 km. We therefore incorporate Fast-JX v7.0a into GEOS-Chem UCX. Fast-JX includes cross-section data for many species relevant to the troposphere and stratosphere. However, accurately representing sulfur requires calculation of gaseous H_2SO_4 photolysis, a reaction which is not present in Fast-JX but which acts as a source of sulfur dioxide in the upper stratosphere. Based on a study by Mills (2005), the mean cross-section between 412.5 and 850 nm is estimated at 2.542×10^{-25} cm^2. We also add photolysis of ClOO and $ClNO_2$, given their importance in catalytic ozone destruction, using data from JPL 10-06 (Sander et al., 2011). Fast-JX v7.0a includes a correction to calculated acetone cross sections. Accordingly, where hydroxyacetone cross-sections were previously estimated based on one branch of the acetone decomposition, a distinct set of cross sections from JPL 10-06 are used.

The base version of GEOS-Chem uses satellite observations of total ozone columns when determining ozone-related scattering and extinction. The UCX allows either this approach, as was used for the production of the results shown, or can employ calculated ozone mixing ratios instead, allowing photolysis rates to respond to changes in the stratospheric ozone layer.

2.1.3. Heterogeneous chemistry

To capture seasonal ozone depletion (Solomon, 1999), eight new heterogeneous reactions are modeled with uptake coefficients and reaction probabilities from GMI (Kirner et al., 2011; Rotman et al., 2001) and JPL 10-06 (Shi et al., 2001). Heterogeneous polar stratospheric cloud (PSC) reactions are considered to be pseudo-first-order, limited to a minimum reactant lifetime of 1 ms. This prevents overshoot while permitting rapid halogen activation upon formation of a suitable reaction surface.

2.2. Stratospheric H_2O

Given the complexity of the tropospheric hydrological cycle, H_2O was left as a passive tracer throughout the troposphere, with mixing ratios derived from GEOS-5 humidity fields. However, within the stratosphere we now treat H_2O as a chemically-active advected tracer. The UCX can therefore respond to events such as dehydration through sedimentation of ice PSCs. The model can be initialized based on the existing meteorological data if distributions from a previous simulation are not available, to ensure reasonable initial conditions. Alternatively, this feature can be deactivated in the model options.

2.3. Aerosols

Two new aerosols are implemented, split into stratospheric particulate (solid) and liquid aerosol (SPA and SLA). The former consists of type Ib and type II PSCs, made up of nitric acid trihydrate (NAT) and ice. The latter covers all stratospheric sulfate aerosols, ranging from H_2SO_4 liquid binary solutions (LBS) to supercooled ternary solution (STS) with parameterized uptake of HNO_3, $ClNO_3$, HOCl, HCl, $BrNO_3$, HOBr and HBr (Carslaw et al., 1997).

Stratospheric aerosol formation is modeled on a recent implementation in ECHAM-MESSy (Kirner et al., 2011). Available H_2SO_4 is calculated by assuming that all stratospheric sulfates take the form of sulfuric acid, using a phase partitioning parameterization (Kulmala and Laaksonen, 1990). This results in gas phase H_2SO_4 above approximately 35 km and condensed liquid aerosol below. Interpolation is applied over 0.01 μPa to prevent unphysical behavior arising from spatial discretization, with only gas-phase H_2SO_4 available for photolysis. Uptake of HNO_3 and trace halogens into the liquid aerosol is calculated according to Carslaw et al. (1997) using grid box mean aerosol conversion parameters calculated from Grainger et al. (1995). As the temperature falls, HNO_3 uptake is promoted, resulting in STS formation. At lower temperatures still, this HNO_3 "freezes out" to form NAT. This process is modeled by calculating NAT formation prior to calculating HNO_3 uptake into STS, removing HNO_3 from the liquid into the solid phase. NAT forms either heterogeneously on existing solid PSCs or homogeneously with a supercooling criterion of 3 K below the vapor saturation temperature. Homogeneous NAT nucleation can be disabled, and was not employed for the simulations below. Aqueous-phase reaction rates are calculated based on JPL 10-06 (Hanson, 2003; Sander et al., 2011; Shi et al., 2001).

Stratospheric aerosols are modeled in thermodynamic equilibrium. Physical properties are recalculated based on local temperature, pressure and mixing ratios. If no particles already exist in a given grid cell, a 20% supersaturation ratio is required before solid PSC formation is permitted. This approximates a model of PSC formation whereby ice particles form homogeneously, followed by NAT condensing onto the surface. When calculating surface reaction probabilities (γ), the surface is assumed to be NAT if there is any NAT present in the grid cell. A kinetic aerosol growth parameterization, which will allow aerosol evolution and persistence, is to be implemented in future work. However, the current parameterization is fast and allows calculation of approximate surface area densities for heterogeneous chemistry while also permitting PSC denitrification and dehydration. Effective aerosol radii are estimated for optical depth calculations, allowing stratospheric aerosols to affect both stratospheric and tropospheric photochemistry. Scattering and absorption parameters for SLA are based on stratospheric background sulfate, with irregular ice cloud properties used for SPA. Relevant optical data are already present in GEOS-Chem.

The new stratospheric aerosol formation mechanism replaces ISORROPIA II above the tropopause, such that ammonium is ignored and allowed to advect freely if it reaches the stratosphere. High altitude emissions from aviation and volcanoes, which were simplified or removed above the tropopause in the base model, now take place with no restrictions.

Gravitational settling of stratospheric soot and sulfates is calculated using Stokes' law with a slip correction factor. Trace species taken up into aerosols are also sedimented. SPA are sedimented using a trapezoidal scheme which accounts for non-uniform vertical particle number density profiles within individual grid boxes by estimating the location of aerosol number density maxima and minima (Buchholz, 2005).

2.4. Surface emissions and boundary conditions

Emissions of biogenic bromine species were implemented in GEOS-Chem prior to the UCX (Parrella et al., 2012). A fixed global surface mixing ratio boundary condition is applied for N_2O, CFCs, HCFCs, halons, OCS and long-lived organic chlorine species, using

500 pptv for OCS (Weisenstein et al., 1997) and monthly WMO values (Daniel et al., 2007) for the others.

The base model contains a methane emissions inventory for use in offline methane-only simulations with prescribed OH (EC-JRC, 2009; Fung et al., 1991; Pickett-Heaps et al., 2011; Van der Werf et al., 2010; Yevich and Logan, 2003). This inventory is now used in place of the fixed zonal average methane fields previously employed by GEOS-Chem. The estimated annual methane emissions fluctuate depending on soil wetness, but the total emissions are approximately 470 Tg/yr before soil uptake is taken into account. Alternatively, setting a switch in the UCX input menu will replace methane emissions with a surface boundary condition, ensuring that the atmospheric methane mixing ratios stay close to projected values at the expense of model flexibility.

2.5. Mesospheric treatment

The chemical mechanism is limited to 0.1 hPa, preventing explicit calculation of mesospheric chemistry. Species with super-stratospheric sinks may therefore form non-physical reservoirs, which could disrupt chemistry elsewhere. To prevent this, we employ a simple high-altitude NO_y mechanism. Based on zonal mean $O(^3P)$, $O(^1D)$ and J-rates taken from a 2D model (Weisenstein et al., 1997), NO_x and N_2O are destroyed, producing molecular nitrogen and removing active nitrogen above the stratosphere. Similarly, H_2SO_4 photolysis to convert mesospheric sulfates to sulfur dioxide is simulated by propagating the H_2SO_4 J-rate upwards from the stratopause in a separate calculation. For all other species, we employ relaxation to climatology throughout the mesosphere, as was previously employed in both the mesosphere and stratosphere.

We do not consider Lyman-Alpha line photochemistry or mesospheric chemical sources such as solar proton events and photodissociation of molecular nitrogen. This may result in an underestimation of upper stratospheric NO_x (Jackman et al., 1980), but we leave the modeling of such effects as a future research aim.

3. Evaluation

To verify the ability of the UCX to accurately model Earth's atmosphere chemistry, we present results from four simulation years. We first intercompare results from base GEOS-Chem and the UCX to demonstrate that implementation of stratospheric chemistry has not impaired tropospheric modeling (which has already been extensively validated). We then assess GEOS-Chem UCX's ability to reproduce the atmosphere when compared to other models and historical observations. Finally, we estimate source gas stratospheric lifetimes and their correlations with active species.

3.1. Model setup

Both the base and extended model were initialized with identical atmospheric loading of common species. For new species, initial distributions were taken from the AER 2-D chemistry-transport model (Weisenstein et al., 1997). The only exceptions were H_2O, which was initialized according to meteorological data, and stratospheric NO_y and sulfates, which are initialized from 2D data in the UCX. Methane was left as a prescribed field for the base model, while the UCX employed the methane boundary condition described in Section 2.4. Both models were driven using GEOS-5 meteorological inputs on the same underlying model grids with identical emission inventories for common species. Simulations ran for 2004–2007 at a horizontal resolution of $4^\circ \times 5^\circ$. This resolution was chosen to minimize run time, in light of the eight-fold simulation time increase resulting from each doubling of spatial resolution. Although we did not perform an exhaustive timing analysis, the models were run on physically identical hardware and the UCX simulation completed in approximately 160% the time of the base simulation without code optimization. This level of performance suggests that maintaining a single unified version of GEOS-Chem is practical (rather than long-term use of branched unified and tropospheric versions).

3.2. Comparison to GEOS-Chem v9-01-03

3.2.1. Tropospheric hydroxyl (OH) radical

Historically, global CTMs have been compared based on the estimated mean tropospheric hydroxyl radical (OH) concentration. Here, we take the approach recommended by Lawrence et al. (2001), weighting grid box OH concentrations by air mass to calculate mean OH for each of 12 regions. We compare these results to climatology (Spivakovsky et al., 2000) and a multi-model analysis by Naik et al. (2013). The results are shown in Fig. 1.

The base and extended model OH are equal to within 4% in all 12 regions. Global mean OH and estimated CH_4 lifetimes against destruction by OH were calculated using air-mass weightings recommended by Lawrence et al. (2001), averaging daily means from the target year. The relevant reaction rate is calculated based on JPL 10-06.

UCX increased global mean OH from 11.9×10^5 to 12.0×10^5 molec/cm^3. The primary OH generation mechanism is more detailed, with OH generation from $O(^1D) + H_2O$ calculated explicitly rather than assuming photochemical steady-state. This results in increased atmospheric oxidizing power, reducing mean CH_4 lifetime from 7.27 to 7.20 years compared to Spivakovsky's 8.23 years. Naik et al. (2013) found a multi-model mean global OH of $11.12 \pm 1.6 \times 10^5$ molec/cm^3. Although the UCX results are within this range, already high OH concentrations have been slightly increased by the implementation of online stratospheric chemistry. Moving to the regional distribution, the UCX has increased mean OH in all 12 regions by 1–4%. This discrepancy is greatest in the extreme southern latitudes. An analysis of trends in CH_3CCl_3 by Prinn et al. (2001) estimated that southern hemispheric (SH) OH concentrations are 14 $\pm$ 35% greater than those in the northern hemisphere (NH). The base model finds the difference to be −25.2%, compared to −23.7% in the UCX and −28% from the multi-model analysis. The UCX therefore does not affect the pre-existing problem of models overestimating relative NH to SH OH production. It should be noted that these results are sensitive to the chosen meteorological data and sampling period.

3.2.2. Surface-level effects

The mean mixing ratio from the simulation period was calculated for each surface grid cell in GEOS-Chem and the UCX, isolating the largest discrepancy. Of the 53 tracers present in the base model, the absolute mean difference is within 5% for most tracers. The exceptions are nitrogen species and bromine species. Peroxypropionyl nitrates (PPN) and nitrate aerosols (specifically the NO_3^- ion) show maximum variations between 5 and 10%, likely the result of changes in the photolysis code resulting in adjusted NO_x partitioning. However, the balance of inorganic aerosols is maintained, with variations of both NH_4^+ and SO_4^{2-} below 5%. Of the bromine species, Br and HBr variations are between 5 and 10%, while $BrNO_2$ and $BrONO_2$, which are sensitive to both nitrogen and bromine partitioning, show maximum variations of 10.6 and 22.4% respectively. There are two likely causes of this. Firstly, the changes in OH and photolysis rates affect the partitioning of both bromine and nitrogen, which coupling species will be particularly sensitive to. Secondly, implementation of the UCX included a fix for the CH_3Br

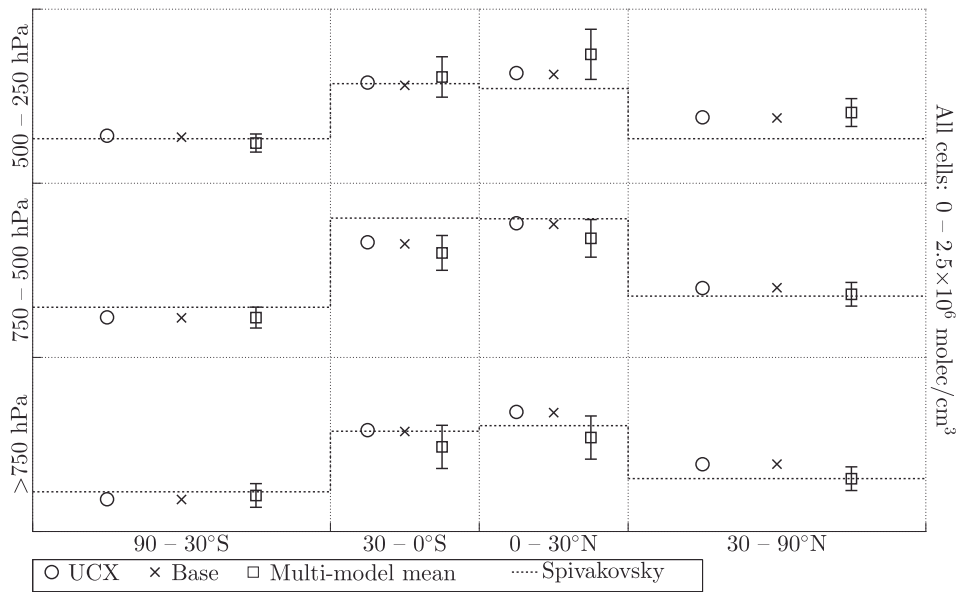

Fig. 1. Comparison of air mass-weighted model OH to results from a multi-model mean (Naik et al., 2013) and a reference climatology (Spivakovsky et al., 2000). The vertical limits on each box range from 0 to 2.5 × 10^6 molec/cm^3 on a linear scale. Data for both versions of GEOS-Chem are annual means for 2007.

boundary condition which increases the available bromine at the surface by approximately 7–8 pptv.

3.3. Stratospheric chemistry

3.3.1. Global ozone distribution

The ozone layer is a key feature of the stratosphere dependent on a large number of stratospheric processes including halogen cycles, aerosol formation and short-wavelength photochemistry. We use it to demonstrate the improved stratospheric modeling of the UCX. Fig. 2 compares column ozone estimates from the base model's monthly-mean relaxation scheme, the UCX online calculations and observations by the Total Ozone Mapping Spectrometer (TOMS), respectively. Fig. 3 shows the zonal mean and range for each in 2007, highlighting the extent of the correlation between base and UCX results at midlatitudes and suggesting that the new online chemistry reliably replicates results previously achieved through relaxation to a known climatology. However, during Southern hemispheric winter the UCX exhibits formation of an Antarctic ozone hole which is not well replicated by the base

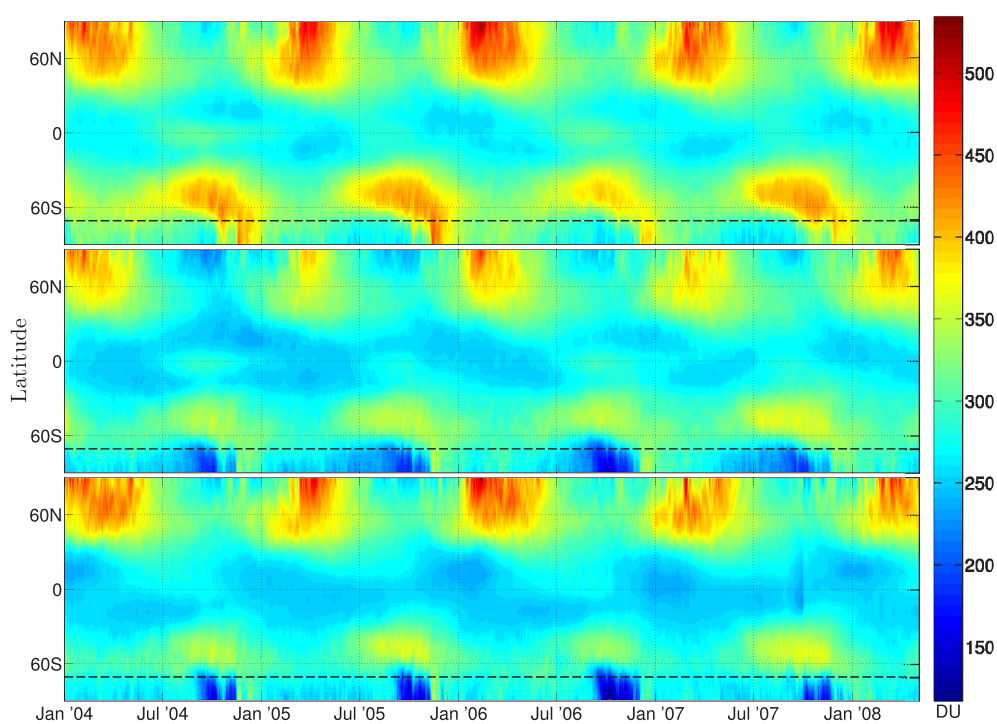

Fig. 2. Zonal-mean column ozone for 2004–2007 from the base model (top), UCX (middle) and TOMS data (bottom). Model results are shown in terms of odd oxygen to allow fair intercomparison. The dashed line corresponds to Neumayer station, from which ozonesonde measurements were used in Section 3.3.2.

model. Ozone depletion over the Antarctic influences the rest of the southern hemisphere after the breakdown of the polar vortex each spring. The chemistry local to the ozone hole is explored more thoroughly in Section 3.3.2. The overall column ozone discrepancy has been reduced globally from 9.9% to 3.6% through the addition of the UCX, based on the area-weighted mean absolute difference of the values shown in Fig. 3.

Following Emmons et al. (2010), ozonesonde data was obtained from the World Ozone and Ultraviolet radiation Data Center (WOUDC, retrieved 5th September 2013 from http://www.woudc.org) and compared to model results. Further information is given in the SI. Results were binned by latitude based on launch location, using the same boundaries as for the OH analysis in Section 3.2.1. Vertically, samples were averaged in four regions defined by pressure boundaries. Three were tropospheric, using the same boundaries as in the MOZART-4 evaluation at ±100 hPa around 900 hPa, 650 hPa and 400 hPa. The final bin was chosen to demonstrate stratospheric ozone behavior, bounded at 30–5 hPa. The samples were weighted uniformly and averaged by month and year. Comparison data were averaged from the nearest grid box, weighted uniformly to account for bias resulting from the non-uniform frequency and spacing of the measurements. The full comparison is shown in Fig. 4 with root mean square coefficient of variation (CV) and mean bias ($\Delta\mu$) given for each bin.

The mean bias is within ±10% for 13 of the 16 zones and ±17% globally. The stratospheric band not used by Emmons et al. shows the greatest variation between the UCX and base model. The model spinup process is clearly shown as the UCX exhibits low ozone mixing ratios throughout the first 3 years, during which the stratospheric air is going through its first turnover. The base model, relaxing to climatological means rather than calculating ozone mixing ratios online, does not suffer from such a spinup problem. However, by the final simulation year, the UCX simulation shows mixing ratios that are closer to the TOMS observations at all latitudes except the southern midlatitudes.

Moving to the tropospheric results, at high Northern latitudes the model underestimates ozone recovery during polar springtime in the upper troposphere, resulting in errors between −15% and −25% and a mean bias of −5.37%. Arctic ozone depletion shows finer spatial and temporal structure than in the Antarctic, with greater local variability associated with atmospheric waves (Solomon, 1999). Since GEOS-Chem averages over 'polar caps' beyond ±84° to compensate for artificial polar singularities resulting from a global longitude–latitude grid, such fine structure is lost, resulting in the reduced variability. (This will be rectified in an upcoming grid-independent version of GEOS-Chem.) Stratospheric ozone depletion is also highly sensitive to aerosol loadings. The thermodynamic equilibrium model for aerosol and PSC formation underestimates ozone variability in regions with rapid temperature fluctuations.

The negative bias observed elsewhere is reversed at high southern latitudes, with a mean bias of +11.6% in the upper troposphere. Fig. 2 shows that the overall ozone depletion in this region is underestimated. This is explored in detail in Section 3.3.2, but we suggest it is due to the fact that well-mixed Eulerian frameworks cannot effectively isolate the air within the polar vortex.

Underprediction of upper tropospheric Northern ozone remains consistent down to 750 hPa, with an increase in both mean bias, to −8.2%, and variance. This trend is not visible at the surface as high Northern hemispheric surface emissions dominate the impact of the coarsely resolved polar stratosphere. Above 750 hPa in the Northern tropics, the results show low mean biases of the order of +1–3%, and CVs below 1%. The model captures some interannual variation such as the peak in August 2004, but does not register other events such as a large spike in Northern tropical ozone at the end of 2005. This discrepancy propagates to all altitudes, indicative of a specific event. This could be caused by a tropopause folding event bringing stratospheric ozone into the troposphere.

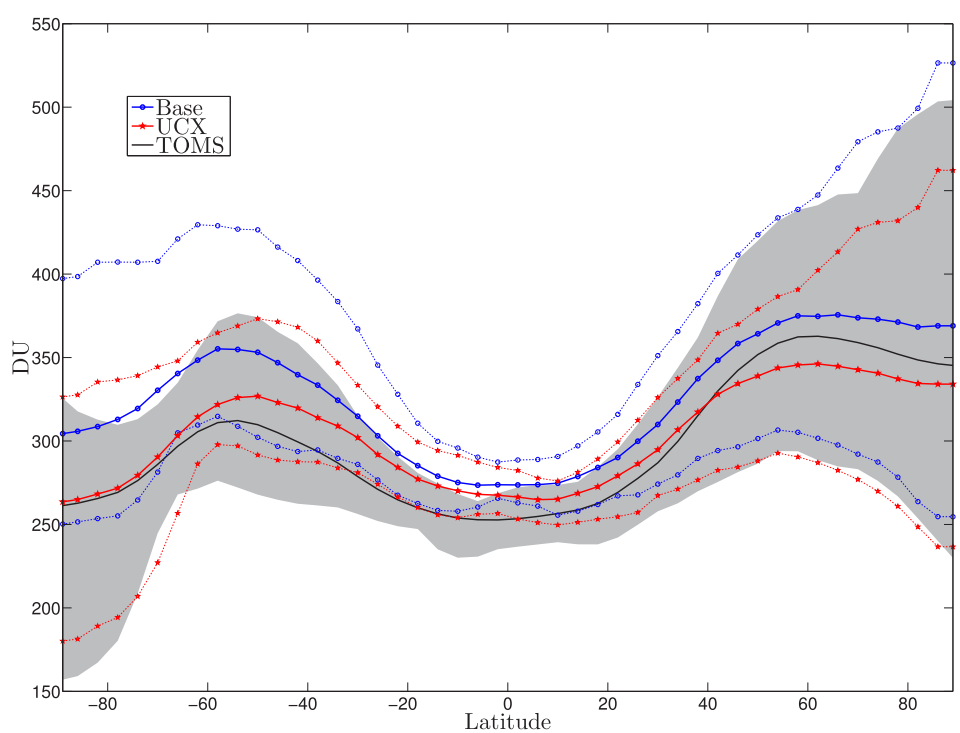

Fig. 3. Mean column ozone in the base model, UCX and TOMS measurements. Solid lines are 2007 means, with the range of measurements from 2007 shown as dotted lines for the model and as a shaded region for TOMS.

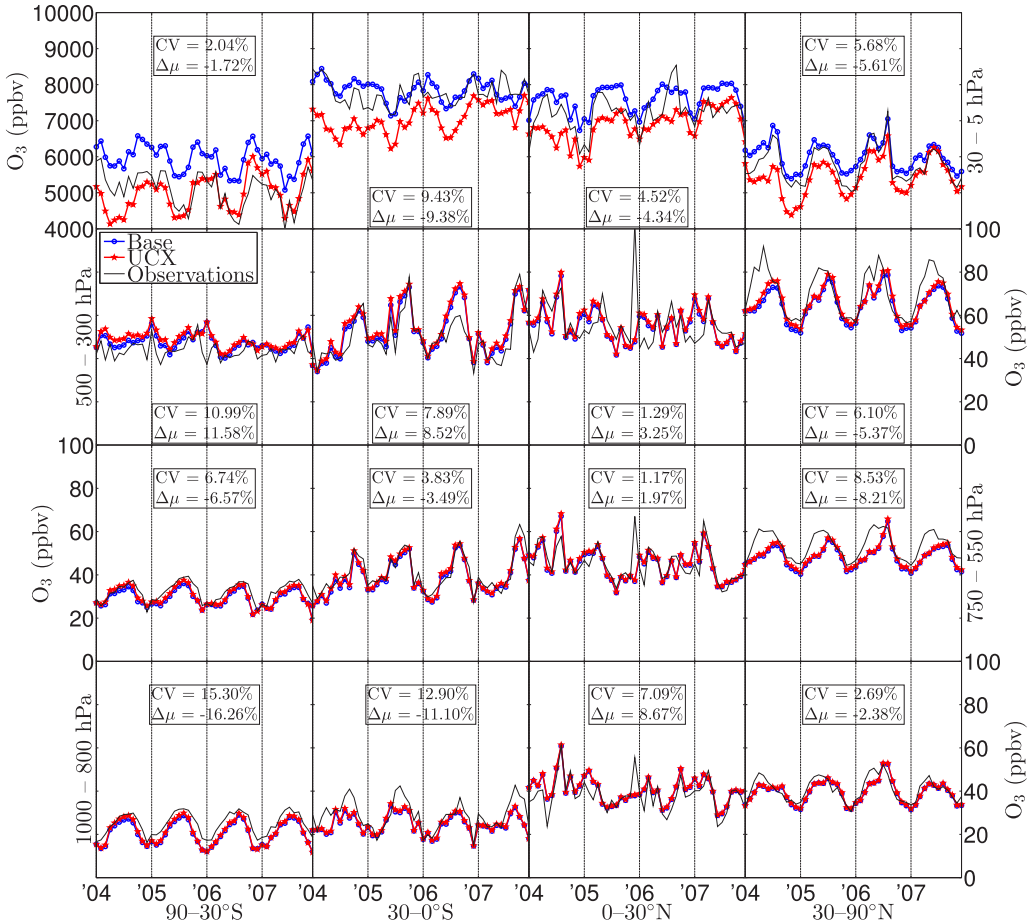

Fig. 4. Comparison of tropospheric ozonesonde data to GEOS-Chem UCX and the base model.

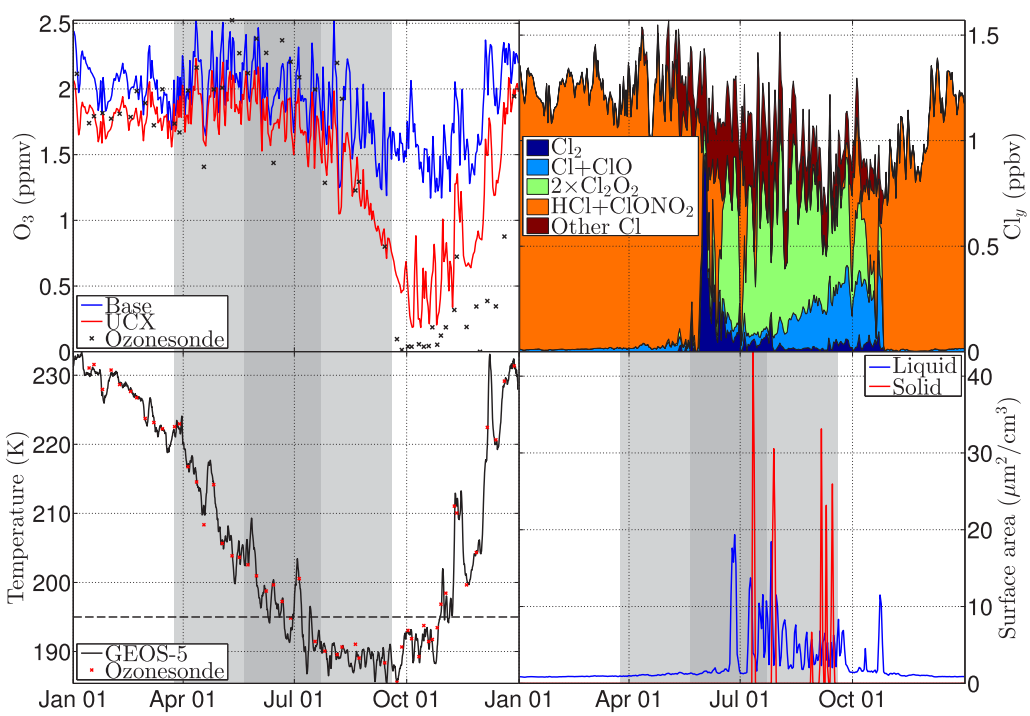

Fig. 5. Clockwise, from top left: ozone burden, inorganic chlorine partitioning, PSC surface area density and temperature for the year 2006 at 73 hPa over Neumayer. The shaded regions correspond to local and polar night, and the dashed line is the typical chlorine activation threshold temperature (Grooß et al., 2011).

3.3.2. Antarctic ozone depletion

The mechanisms underlying stratospheric ozone depletion by chlorine have been extensively investigated and documented since the discovery of the Antarctic ozone hole (Solomon, 1999). These mechanisms involve rapid catalytic cycling, with strong dependence on stratospheric aerosol surface area densities. These in turn are highly sensitive to meteorological conditions. Capturing such depletion requires mechanisms not typically present in tropospheric models, including polar stratospheric cloud (PSC) microphysics and heterogeneous halogen chemistry.

As a test of these features within the UCX, Fig. 5 shows the modeled ozone depletion behavior over 72°S, 10°W for 2006. We chose 2006 due to the extent of the Antarctic ozone hole. This grid box contains the Neumayer observation station (70.65°S, 8.26°W), which supplied ozonesonde data for comparison. A sampling pressure altitude of 73 hPa was chosen on the basis of a recent study investigating rapid ozone depletion which informed our chemical mechanism choices (Grooß et al., 2011). Meteorological conditions including temperature and the extent of local and polar nighttime are also shown. The light shading corresponds to polar nighttime at 89°S, while darker shading corresponds to local nighttime at Neumayer.

Fig. 5 compares modeled ozone depletion to ozonesonde data, showing odd oxygen (O_x) from the base model and ozone from UCX. The base model's chemical mechanism is limited to the troposphere, instead using the Linoz method to solve for ozone and storing the result in the O_x tracer. Taking 2 ppmv as an approximate springtime mean, and recognizing that the ozonesondes show 100% depletion, the extended model achieves an approximate maximum depletion of 90% compared to 40% in the base model.

Although the modeled depletion is 50% greater than the base model, UCX overestimates the rate of ozone recovery beginning around mid-November. By comparison, observations at Neumayer show ongoing depletion until mid-December. This is mirrored by underestimated ozone destruction rates. Observed ozone is near-zero by late September, while the modeled minimum occurs in mid-October. There are two likely causes. Firstly, well-mixed grid boxes in an Eulerian framework compromise the isolation of the polar vortex, which is made worse by the combination of GEOS-Chem's large (84°S and above) averaged polar cap and the low resolution used in these simulations. This degraded isolation results in undepleted extravortical air replenishing the modeled ozone concentrations.

Secondly, the rate of chlorine-based ozone depletion is a function of available ClO_x, which depends on the relative chlorine activation and deactivation rates. Activation occurs through heterogeneous chemistry on PSCs, while gas-phase reactions dominate deactivation (Grooß et al., 2011). Fig. 5 also shows the modeled liquid and solid aerosol surface areas for this period. The thermodynamic aerosol parameterization, coupled with the coarse horizontal resolution that precludes localized PSC formation, will underestimate the overall surface area density (SAD). In reality, aerosols can form in small low-temperature regions and then persist even once local temperatures have exceeded the frost point, but this is not captured in a pure thermodynamic equilibrium model at coarse grid resolutions. This manifests as a cessation in ozone depletion when aerosol loadings return to pre-vortex levels, which in turn occurs immediately after the temperature rises above the approximate PSC formation or "chlorine activation" temperature. Measurements of PSCs by Gobbi et al. (1998) suggest that we should observe SADs of 2–10 $\mu m^2/cm^3$, whereas modeled densities are 0.5–2 $\mu m^2/cm^3$.

This analysis is informed by the total inorganic chlorine (Cl_y) partitioning between molecular chlorine (Cl_2), active chlorine ($Cl + ClO = ClO_x$), the ClO dimer Cl_2O_2, reservoir chlorine in the forms of HCl and $ClONO_2$, and other modeled inorganic chlorine species ($ClOO + OClO + ClNO_2 + HOCl =$ Other Cl). Ozone recovery begins immediately after complete deactivation into reservoir chlorine; based on analysis by Grooß et al. (2011), the modeled unrealistic recovery of ozone is likely due to insufficient reactivation of chlorine which would otherwise balance ongoing chlorine deactivation.

3.3.3. Source gas stratospheric lifetimes

We calculate the stratospheric lifetimes of some tracers for comparison with recent estimates by Brown et al. (2013) based on the ACE-FTS experiment, summarized in Table 2. As recommended in the paper, we linearly scale their results to reflect a lifetime for CFC-11 of 60 years rather than WMO estimates of 45 years, corresponding to estimates by Douglass et al. (2008). The "previous estimates" are referenced from the 2006 and 2010 Scientific Assessments of Ozone Depletion (Daniel et al., 2007; Montzka et al., 2011) and a previous study of stratospheric lifetimes (Volk et al., 1997). The UCX lifetimes are calculated from global burdens and stratospheric removal rates, while the Brown et al. lifetimes are derived from tracer–tracer correlations with CFC-11.

All of the estimated lifetimes lie between the previous estimated lower bound and Brown et al.'s upper bound, apart from CH_3Cl. Both CH_3Cl and CH_4 exhibit stratospheric lifetimes of the order of 50% lower than that estimated by Brown et al. Of the species shown, these are the only two with significant OH reaction branches. As such, their relatively low lifetimes are likely due to the aforementioned high OH.

3.3.4. Correlation studies

Popp et al. (2009) showed a robust correlation between stratospheric ozone and nitric acid (HNO_3), based on in-situ and satellite measurements. We replicate their approach (specifically Popp et al. Fig. 5) in Fig. 6. The smooth lines correspond to polynomial fits based on ACE-FTS interferometry and MLS satellite data. We used daily mean data corresponding to measurements on the same day from the mean location of all measurements for each instrument.

The form of the correlation between the trend in both cases follows the polynomial fit, with HNO_3 peaking at the same ozone mixing ratio as was observed for each of the three observation sites. The MLS data also observed narrow peaks shown in the model, which are not reflected in the polynomial fits. The largest discrepancy is in the MLS equatorial data, although this fit is to a small number of measurements and does not appear to follow the observed trends elsewhere. The explanation by Popp et al. is that air parcels traveling with the Brewer–Dobson circulation evolve from an initial high ozone condition, moving through regions of high

Table 2
Stratospheric lifetime of selected species. Range shown for ACE-FTS corresponds to uncertainty, range for UCX corresponds to absolute range in daily-mean values for 2007.

	Brown et al[a]	GEOS-Chem UCX	Previous estimates
CFC-11	60.0[b] [56.0–64.0]	58.9 [48.9–66.5]	45[c]
CFC-12	150 [127–184]	123 [108–136]	100[c]
CH_3Cl	92.4 [62.4–179]	43.8 [37.9–46.1]	–
CCl_4	46.2 [37.2–61.2]	50.6 [42.1–57.1]	35[c] [26–50]
N_2O	164.4 [127–235]	148 [132–162]	114[d]
CH_4	260 [203.4–359.4]	164 [147–175]	93[e] [75–111]

[a] Brown et al., 2013.
[b] CFC-11 lifetime from Douglass et al., 2008 used to scale other lifetimes.
[c] Montzka et al., 2011.
[d] Daniel et al., 2007.
[e] Volk et al., 1997, based on estimated lifetime for CFC-11 of 45 years.

HNO_3 production to achieve larger HNO_3–O_3 ratios with increasing latitude. The UCX results support this hypothesis, exhibiting evolution of an ozone-rich sample towards a high HNO_3 state with increasing latitude even where the sparsely-populated MLS data is inconclusive. The UCX results depend on the initial conditions selected by the user. In the case of the simulation used to generate these results, the initial stratospheric NO_y distribution increased absolute HNO_3 mixing ratios, resulting in the observed upward bias. Another study by Sankey and Shepherd (2003) compared correlations between stratospheric species in the Canadian Middle Atmosphere Model (CMAM) to data from the ATMOS experiment (Michelsen, 1998). We have recreated Sankey and Shepherd Fig. 14 in our Fig. 7.

The UCX results, unlike those from Sankey and Shepherd, are disperse below 50 hPa. This is especially pronounced in the tropics, suggesting strong tropospheric influence at these altitudes not present in CMAM. The subtropical mixing barrier observed by Michelsen is therefore not well reproduced below 85 hPa. However, at 50 hPa and above, the aforementioned barrier is reflected in a sharp increase of 50–100% in the NO_y/O_3 ratio between the equator and $\pm 30^\circ$, corresponding to the "tropical pipe" transport barrier which separates tropical from extratropical air. Future research may benefit from a dedicated investigation into overrepresentation of tropospheric influence in the GEOS-5 lower stratosphere, since the primary references for this work focus on data above 70 hPa (Fahey et al., 1996; Michelsen, 1998; Murphy et al., 1993). At high southern latitudes in July, the model demonstrates another transport barrier due to the polar vortex.

We also compare NO_y to N_2O, as in Fig. 11 of Sankey and Shepherd (2003) in Fig. 8. Excluding very high altitude sources, N_2O is the only major stratospheric source of NO_y, producing NO through reaction with $O(^1D)$. These species are plotted in Fig. 8. We have successfully reproduced the trend in NO_y relative to N_2O, showing the same consistent maximum of 15–20 ppbv NO_y at 50–70 ppbv N_2O. We also observe the same vertical variation. As altitude increases, N_2O is converted into NO, resulting in the aforementioned peak. The relation's compactness results from both tracers being accurately represented as long-lived compared to the horizontal mixing timescales. The spread in the low altitude Southern Hemispheric data likely results from interference by the polar vortex, with denitrification reducing NO_y mixing ratios at the poles without affecting N_2O. This spread is not visible in CMAM, which does not model denitrification.

4. Conclusions

We have shown here that an online unified chemistry extension can be successfully applied to the GEOS-Chem chemistry-transport model, expanding modeling capabilities and improving the agreement between model and observations without compromising tropospheric chemistry. In particular, we show improved correlation between modeled column ozone and satellite data, capturing

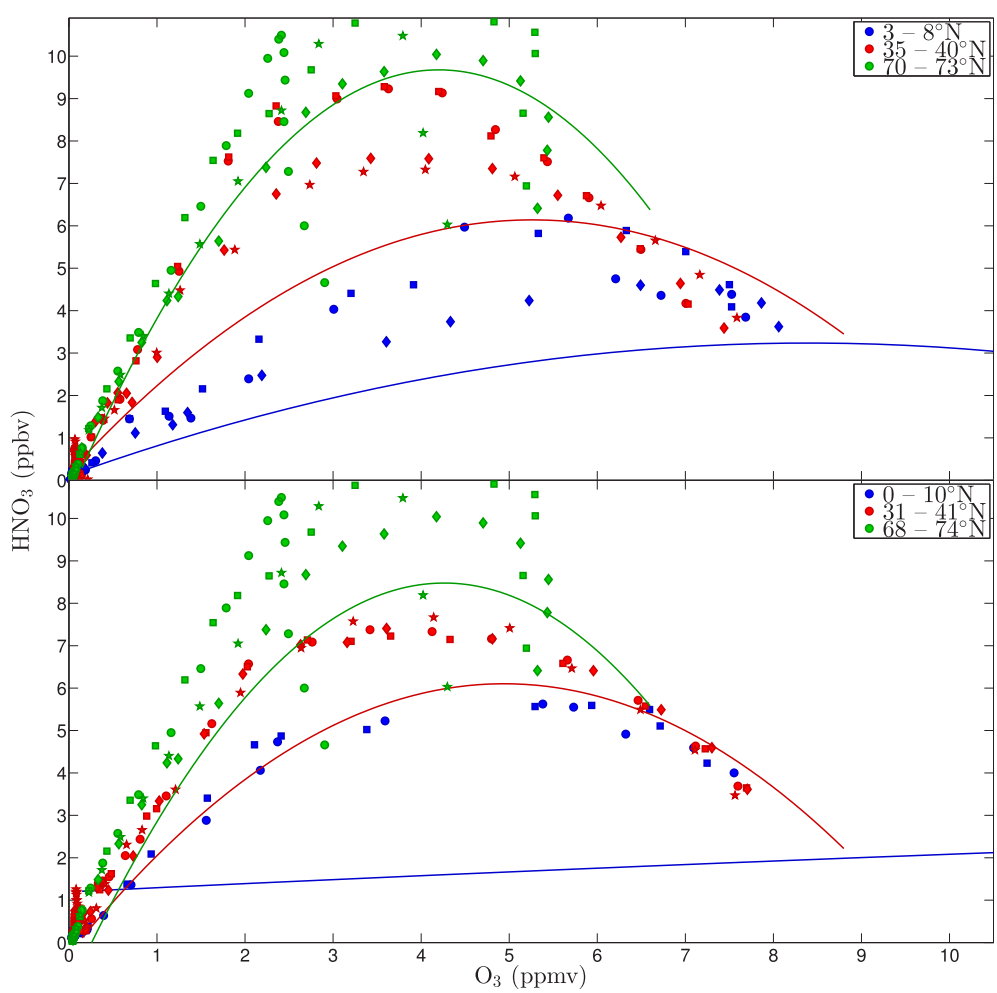

Fig. 6. HNO_3–O_3 correlations in GEOS-Chem UCX (point data) compared to polynomial fits based on measurements from ACE-FTS (top) and MLS (bottom) (Popp et al., 2009). Different markers correspond to different measurement dates.

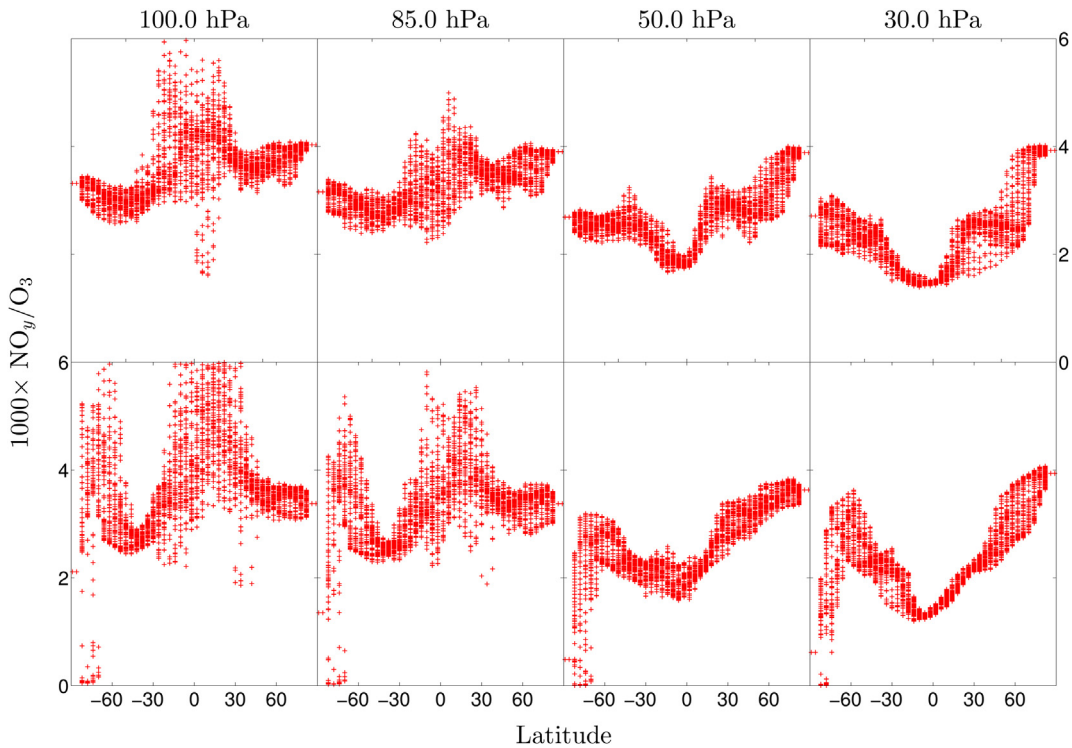

Fig. 7. NO_y/O_3 relations in January (top panel) and July (bottom panel) 2007 from the UCX.

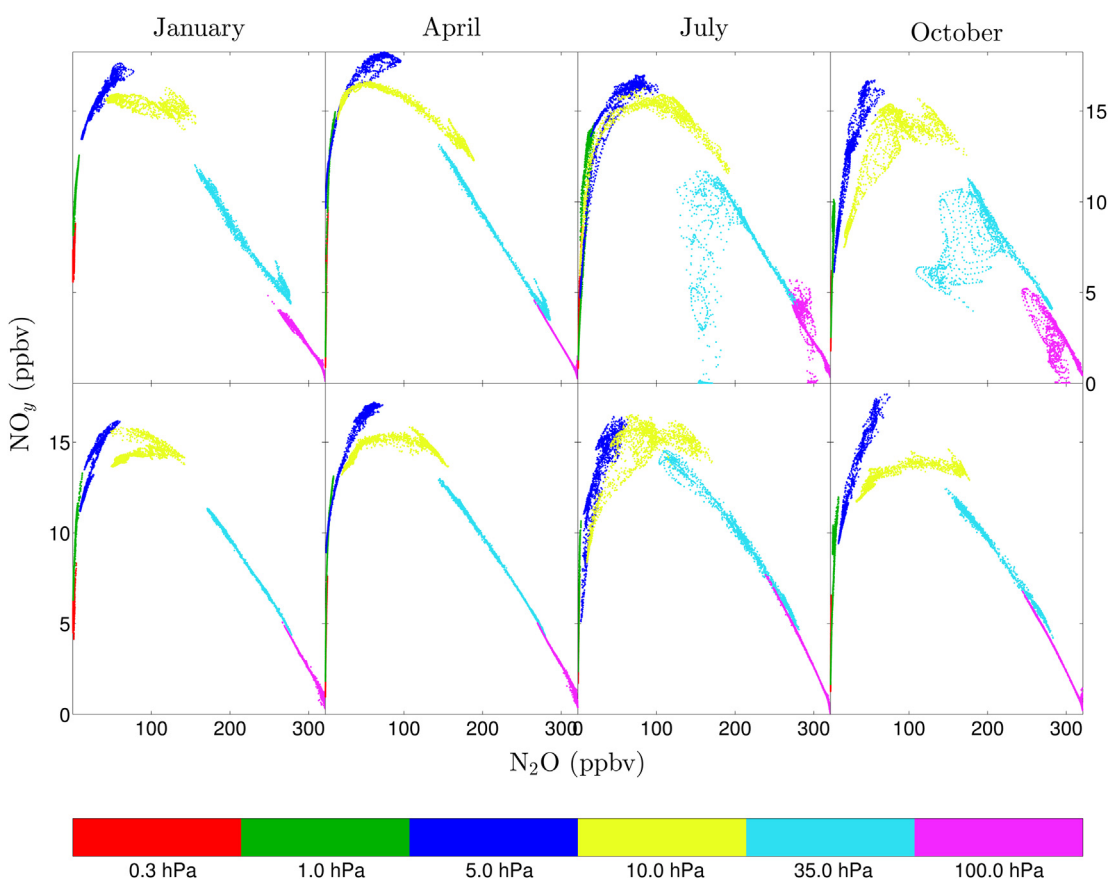

Fig. 8. NO_y versus N_2O throughout the year in the Southern and Northern Hemispheres (top and bottom respectively).

medium- and long-term ozone responses to the Antarctic polar vortex. This was achieved without reducing model stability and only a minimal increase in data requirements in the form of 2-D initial conditions and boundary conditions for stratospheric source gases. Using a thermodynamic aerosol parameterization, we have reproduced ozone depletion trends in southern hemispheric winter. By expanding the wavelength range considered for photolysis calculations, we enabled modeling of stratospheric photochemistry; by combining online radiative transfer calculation in the stratosphere with the aforementioned aerosol parameterization, we have also made it possible to model the potential effects of stratospheric aerosol formation on tropospheric photochemistry through changes in optical depth.

The UCX does not significantly affect the calculated global tropospheric oxidative capacity, resulting in an estimated lifetime of CH_4 against destruction by OH of 7.20 years compared to climatological estimates of around 8.3 years. In particular, we observe zonal seasonal OH means within the range of 80–150% of estimated climatology, although this lies within the calculated zonal seasonal variability of air mass-weighted OH concentrations. This result is also likely to be sensitive to the choice of emissions inventory and meteorological data, which is not investigated here.

Acknowledgments

We would like to thank the many groups and individuals who assisted in developing and validating the GEOS-Chem Unified Chemistry Extension, in particular to Peter Catalfamo now at the MIT Gas Turbine Laboratory who contributed to early prototyping, and Jingqiu Mao's for his implementation of Fast-JX v6.2 in GEOS-Chem. Special thanks go to Daniel Jacob, Lee Murray, Mat Evans, Bob Yantosca and the entire GEOS-Chem team. We thank Susan Solomon for her help in diagnosing and analyzing the model's ozone interactions. We would like also to thank Emmanuel Mahieu, Wuting Yang and Nicholas Deutscher for FTIR data used throughout. We thank Michael Prather for communications regarding Fast-JX. We also acknowledge the science teams involved in production of the World Ozone and Ultraviolet Radiation Data Center (WOUDC) ozonesonde data. Funding was from a Lockheed Martin graduate fellowship, MIT discretionary funds, and a FICER grant.

Appendix A. Supplementary data

Supplementary data related to this article can be found at http://dx.doi.org/10.1016/j.atmosenv.2014.02.001.

References

Arnold, S.R., Chipperfield, M.P., Blitz, M. a, 2005. A three-dimensional model study of the effect of new temperature-dependent quantum yields for acetone photolysis. Journal of Geophysical Research 110, D22305.

Barkley, M.P., Palmer, P.I., Ganzeveld, L., Arneth, A., Hagberg, D., Karl, T., Guenther, A., Paulot, F., Wennberg, P.O., Mao, J., Kurosu, T.P., Chance, K., Müller, J.-F., De Smedt, I., Van Roozendael, M., Chen, D., Wang, Y., Yantosca, R.M., 2011. Can a "state of the art" chemistry transport model simulate Amazonian tropospheric chemistry? Journal of Geophysical Research 116, D16302.

Bey, I., Jacob, D.J., Yantosca, R.M., Logan, J. a., Field, B.D., Fiore, A.M., Li, Q., Liu, H.Y., Mickley, L.J., Schultz, M.G., 2001. Global modeling of tropospheric chemistry with assimilated meteorology: model description and evaluation. Journal of Geophysical Research 106, 23073.

Brown, A.T., Volk, C.M., Schoeberl, M.R., Boone, C.D., Bernath, P.F., 2013. Stratospheric lifetimes of CFC-12, CCl_4, CH_4, CH_3Cl and N_2O from measurements made by the Atmospheric Chemistry Experiment-Fourier Transform Spectrometer (ACE-FTS). Atmospheric Chemistry and Physics 13, 6921–6950.

Buchholz, J., 2005. Simulations of Physics and Chemistry of Polar Stratospheric Clouds with a General Circulation Model. Gutenberg.

Carslaw, K., Peter, T., Clegg, S., 1997. Modeling the composition of liquid stratospheric aerosols. Reviews of Geophysics 35, 125–154.

Chipperfield, M., 2006. The TOMCAT/SLIMCAT Off-line 3D CTM User's Manual.

Considine, D.B., Douglass, a. R., Connell, P.S., Kinnison, D.E., Rotman, D. a., 2000. A polar stratospheric cloud parameterization for the global modeling initiative three-dimensional model and its response to stratospheric aircraft. Journal of Geophysical Research 105, 3955–3973.

Daniel, J.S., Velders, G.J.M., Douglass, A.R., Forster, P.M.D., Hauglustaine, D.A., Isaksen, I.S.A., Kuijpers, L.J.M., McCulloch, A., Wallington, T.J., 2007. Halocarbon scenarios, ozone depletion potentials, and global warming potentials (Chapter 8). In: Scientific Assessment of Ozone Depletion: 2006. World Meteorological Organization, Geneva, Switzerland, p. 572.

De Grandpré, J., Beagley, S.R., Fomichev, V.I., Griffioen, E., McConnell, J.C., Medvedev, A.S., Shepherd, T.G., 2000. Ozone climatology using interactive chemistry: results from the Canadian Middle Atmosphere Model. Journal of Geophysical Research 105, 26475–26491.

Douglass, a. R., Stolarski, R.S., Schoeberl, M.R., Jackman, C.H., Gupta, M.L., Newman, P. a., Nielsen, J.E., Fleming, E.L., 2008. Relationship of loss, mean age of air and the distribution of CFCs to stratospheric circulation and implications for atmospheric lifetimes. Journal of Geophysical Research 113, D14309.

Duncan Fairlie, T., Jacob, D.J., Park, R.J., 2007. The impact of transpacific transport of mineral dust in the United States. Atmospheric Environment 41, 1251–1266.

Emmons, L.K., Walters, S., Hess, P.G., Lamarque, J.-F., Pfister, G.G., Fillmore, D., Granier, C., Guenther, A., Kinnison, D., Laepple, T., Orlando, J., Tie, X., Tyndall, G., Wiedinmyer, C., Baughcum, S.L., Kloster, S., 2010. Description and evaluation of the Model for OZone and Related chemical Tracers, version 4 (MOZART-4). Geoscientific Model Development 3, 43–67.

European Commission, J.R.C. (JRC)/Netherlands E.A.A. (PBL), 2009. Emissions Database for Global Atmospheric Research (EDGAR). Release version 4.0 [WWW Document]. URL. http://edgar.jrc.ec.europa.eu/.

Fahey, D., Donnelly, S., Keim, E., Gao, R., Wamsley, R., Del Negro, L., Woodbridge, E., Proffitt, M., Rosenlof, K., Ko, M., Weisenstein, D., Scott, C., Nevison, C., Solomon, S., Chan, K., 1996. In situ observations of NO_y, O_3, and the NO_y/O_3 ratio in the lower stratosphere. Geophysical Research Letters 23, 1653–1656.

Fung, I., John, J., Lerner, J., 1991. Three-dimensional model synthesis of the global methane cycle. Journal of Geophysical Research 96.

Gobbi, G.P., Di Donfrancesco, G., Adriani, A., 1998. Physical properties of stratospheric clouds during the Antarctic winter of 1995. Journal of Geophysical Research 103, 10859–10873.

Grainger, R.G., Lambert, A., Rodgers, C.D., Taylor, F.W., 1995. Stratospheric aerosol effective radius, surface area and volume estimated from infrared measurements. Journal of Geophysical Research 100, 16507–16518.

Grooß, J.-U., Brautzsch, K., Pommrich, R., Solomon, S., Müller, R., 2011. Stratospheric ozone chemistry in the Antarctic: what determines the lowest ozone values reached and their recovery? Atmospheric Chemistry and Physics 11, 12217–12226.

Hanson, D.R., 2003. Reactivity of $BrONO_2$ and HOBr on sulfuric acid solutions at low temperatures. Journal of Geophysical Research 108, 4239.

Huijnen, V., Williams, J., van Weele, M., van Noije, T., Krol, M., Dentener, F., Segers, a., Houweling, S., Peters, W., de Laat, J., Boersma, F., Bergamaschi, P., van Velthoven, P., Le Sager, P., Eskes, H., Alkemade, F., Scheele, R., Nédélec, P., Pätz, H.-W., 2010. The global chemistry transport model TM5: description and evaluation of the tropospheric chemistry version 3.0. Geoscientific Model Development 3, 445–473.

Jackman, C.H., Frederick, J.E., Stolarski, R.S., 1980. Production of odd nitrogen in the stratosphere and Mesosphere: an intercomparison of source strengths. Journal of Geophysical Research 85.

Kinnison, D.E., Brasseur, G.P., Walters, S., Garcia, R.R., Marsh, D.R., Sassi, F., Harvey, V.L., Randall, C.E., Emmons, L., Lamarque, J.F., Hess, P., Orlando, J.J., Tie, X.X., Randel, W., Pan, L.L., Gettelman, A., Granier, C., Diehl, T., Niemeier, U., Simmons, a. J., 2007. Sensitivity of chemical tracers to meteorological parameters in the MOZART-3 chemical transport model. Journal of Geophysical Research 112, 1–24. file:///home/seastham/Dropbox/Thesis/Reference.

Kirner, O., Ruhnke, R., Buchholz-Dietsch, J., Jöckel, P., Brühl, C., Steil, B., 2011. Simulation of polar stratospheric clouds in the chemistry-climate-model EMAC via the submodel PSC. Geoscientific Model Development 4, 169–182.

Kulmala, M., Laaksonen, A., 1990. Binary nucleation of water–sulfuric acid system: comparison of classical theories with different H_2SO_4 saturation vapor pressures. Journal of Chemical Physics 93, 696.

Lamarque, J.-F., Emmons, L.K., Hess, P.G., Kinnison, D.E., Tilmes, S., Vitt, F., Heald, C.L., Holland, E. a., Lauritzen, P.H., Neu, J., Orlando, J.J., Rasch, P.J., Tyndall, G.K., 2012. CAM-chem: description and evaluation of interactive atmospheric chemistry in the Community Earth System Model. Geoscientific Model Development 5, 369–411.

Lawrence, M.G., Jöckel, P., von Kuhlmann, R., 2001. What does the global mean OH concentration tell us? Atmospheric Chemistry and Physics, 37–49.

Mao, J., Jacob, D.J., Evans, M.J., Olson, J.R., Ren, X., Brune, W.H., Clair, J.M. St, Crounse, J.D., Spencer, K.M., Beaver, M.R., Wennberg, P.O., Cubison, M.J., Jimenez, J.L., Fried, a., Weibring, P., Walega, J.G., Hall, S.R., Weinheimer, a. J., Cohen, R.C., Chen, G., Crawford, J.H., McNaughton, C., Clarke, a. D., Jaeglé, L., Fisher, J. a., Yantosca, R.M., Le Sager, P., Carouge, C., 2010. Chemistry of hydrogen oxide radicals (HO_x) in the arctic troposphere in spring. Atmospheric Chemistry and Physics 10, 5823–5838.

McLinden, C.A., Olsen, S.C., Hannegan, B.J., Wild, O., Prather, M.J., Sundet, J., 2000. Stratospheric ozone in 3-D models: a simple chemistry and the cross-tropopause flux. Journal of Geophysical Research Atmospheres 105 (D11), 14653–14665.

Michelsen, H.A., 1998. Correlations of Stratospheric Abundances of NO_y, O_3, NO, and CH_4 Derived from ATMOS Measurements, vol. 103.

Mills, M.J., 2005. Photolysis of sulfuric acid vapor by visible light as a source of the polar stratospheric CN layer. Journal of Geophysical Research 110, D08201.
Montzka, S.A., Reimann, S., Engel, A., Krüger, K., O'Doherty, S., Sturges, W.T., Blake, D., Dorf, M., Fraser, P., Froidevaux, L., Jucks, K., Kreher, K., Kurylo, M.J., Mellouki, A., Miller, J., Nielsen, O.-J., Orkin, V.L., Prinn, R.G., Rhew, R., Santee, M.L., Stohl, A., Verdonik, D., 2011. Ozone-depleting substances (ODSs) and related chemicals. In: Scientific Assessment of Ozone Depletion: 2010. World Meteorological Organization, Geneva, Switzerland.
Murphy, D.M., Fahey, D.W., Proffitt, M.H., Liu, S.C., Chan, K.R., Eubank, C.S., Kawa, S.R., Kelly, K.K., 1993. Reactive nitrogen and its correlation with ozone in the lower stratosphere and upper troposphere. Journal of Geophysical Research 98, 8751.
Murray, L.T., Jacob, D.J., Logan, J. a., Hudman, R.C., Koshak, W.J., 2012. Optimized regional and interannual variability of lightning in a global chemical transport model constrained by LIS/OTD satellite data. Journal of Geophysical Research 117.
Naik, V., Voulgarakis, a., Fiore, a. M., Horowitz, L.W., Lamarque, J.-F., Lin, M., Prather, M.J., Young, P.J., Bergmann, D., Cameron-Smith, P.J., Cionni, I., Collins, W.J., Dalsøren, S.B., Doherty, R., Eyring, V., Faluvegi, G., Folberth, G. a., Josse, B., Lee, Y.H., MacKenzie, I. a., Nagashima, T., van Noije, T.P.C., Plummer, D. a., Righi, M., Rumbold, S.T., Skeie, R., Shindell, D.T., Stevenson, D.S., Strode, S., Sudo, K., Szopa, S., Zeng, G., 2013. Preindustrial to present-day changes in tropospheric hydroxyl radical and methane lifetime from the Atmospheric Chemistry and Climate Model Intercomparison Project (ACCMIP). Atmospheric Chemistry and Physics 13, 5277–5298.
Parrella, J.P., Jacob, D.J., Liang, Q., Zhang, Y., Mickley, L.J., Miller, B., Evans, M.J., Yang, X., Pyle, J. a., Theys, N., Van Roozendael, M., 2012. Tropospheric bromine chemistry: implications for present and pre-industrial ozone and mercury. Atmospheric Chemistry and Physics 12, 6723–6740.
Pickett-Heaps, C. a., Jacob, D.J., Wecht, K.J., Kort, E. a., Wofsy, S.C., Diskin, G.S., Worthy, D.E.J., Kaplan, J.O., Bey, I., Drevet, J., 2011. Magnitude and seasonality of wetland methane emissions from the Hudson Bay Lowlands (Canada). Atmospheric Chemistry and Physics 11, 3773–3779.
Popp, P.J., Marcy, T.P., Gao, R.S., Watts, L. a., Fahey, D.W., Richard, E.C., Oltmans, S.J., Santee, M.L., Livesey, N.J., Froidevaux, L., Sen, B., Toon, G.C., Walker, K. a., Boone, C.D., Bernath, P.F., 2009. Stratospheric correlation between nitric acid and ozone. Journal of Geophysical Research 114, D03305.
Prather, M.J., 2012. Fast-JX v7.0a (WWW Document).
Prinn, R.G., Huang, J., Weiss, R.F., Cunnold, D.M., Fraser, P.J., Simmonds, P.G., McCulloch, A., Harth, C., Salameh, P., O'Doherty, S., Wang, R.H., Porter, L., Miller, B.R., 2001. Evidence for substantial variations of atmospheric hydroxyl radicals in the past two decades. Science 292, 1882–1888.
Rotman, D., Tannahill, J., 2001. Global modeling initiative assessment model – model description, integration, and testing of the transport shell. Journal of Geophysical Research 106, 1669–1691.
Rotman, D.A., Tannahill, J.R., Kinnison, D.E., Connell, P.S., Bergmann, D., Proctor, D., Rodriguez, J.M., Lin, S.J., Rood, R.B., Prather, M.J., Rasch, P.J., Considine, D.B., Ramaroson, R., Kawa, S.R., 2001. Global modeling initiative assessment model: model description, integration, and testing of the transport shell. Journal of Geophysical Research 106, 1669–1691.
Sander, S.P., Friedl, R.R., Barker, J.R., Golden, D.M., Kurylo, M.J., Sciences, G.E., Wine, P.H., Abbatt, J.P.D., Burkholder, J.B., Kolb, C.E., Moortgat, G.K., Huie, R.E., Orkin, V.L., 2011. Chemical Kinetics and Photochemical Data for Use in Atmospheric Studies Evaluation Number 17 NASA Panel for Data Evaluation.
Sankey, D., Shepherd, T.G., 2003. Correlations of long-lived chemical species in a middle atmosphere general circulation model. Journal of Geophysical Research 108, 4494.
Shi, Q., Jayne, J., Kolb, C., Worsnop, D., Davidovits, P., 2001. Kinetic model for reaction of $ClONO_2$ with H_2O and HCl and HOCl with HCl in sulfuric acid solutions. Journal of Geophysical Research 106, 24259–24274.
Solomon, S., 1999. Stratospheric ozone depletion: a review of concepts and history. Reviews of Geophysics, 275–316.
Søvde, O. a., Prather, M.J., Isaksen, I.S. a., Berntsen, T.K., Stordal, F., Zhu, X., Holmes, C.D., Hsu, J., 2012. The chemical transport model Oslo CTM3. Geoscientific Model Development 5, 1441–1469.
Spivakovsky, C.M., Logan, J. a., Montzka, S. a., Balkanski, Y.J., Foreman-Fowler, M., Jones, D.B. a., Horowitz, L.W., Fusco, a. C., Brenninkmeijer, C. a. M., Prather, M.J., Wofsy, S.C., McElroy, M.B., 2000. Three-dimensional climatological distribution of tropospheric OH: update and evaluation. Journal of Geophysical Research 105, 8931.
Van der Werf, G.R., Randerson, J.T., Giglio, L., Collatz, G.J., Mu, M., Kasibhatla, P.S., Morton, D.C., DeFries, R.S., Jin, Y., van Leeuwen, T.T., 2010. Global fire emissions and the contribution of deforestation, savanna, forest, agricultural, and peat fires (1997–2009). Atmospheric Chemistry and Physics 10, 11707–11735.
Volk, C., Elkins, J., Fahey, D., Dutton, G., Gilligan, J., Loewenstein, M., Podolske, J., Chan, K., Gunson, M., 1997. Evaluation of source gas lifetimes from stratospheric observations. Journal of Geophysical Research 102, 25543–25564.
Weisenstein, D.K., Yue, G.K., Ko, M.K.W., Sze, N.-D., Rodriguez, J.M., Scott, C.J., 1997. A two-dimensional model of sulfur species and aerosols. Journal of Geophysical Research 102.
Wild, O., Zhu, X., Prather, M., 2000. Fast-J: accurate simulation of in- and below-cloud photolysis in tropospheric chemical models. Journal of Atmospheric Chemistry, 245–282.
Yevich, R., Logan, J.A., 2003. An assessment of biofuel use and burning of agricultural waste in the developing world. Global Biogeochemical Cycles 17 (4), 1095. http://dx.doi.org/10.1029/2002GB001952.